

FSC: Few-point Shape Completion

Xianzu Wu^{1,3*}, Xianfeng Wu^{1*}, Tianyu Luan², Yajing Bai¹, Zhongyuan Lai^{1†}, Junsong Yuan²

¹State Key Laboratory of Precision Blasting, Jiangnan University, Wuhan, 430056

²Department of Computer Science and Engineering, University at Buffalo, Buffalo, New York 14260

³School of Geophysics and Petroleum Resources, Yangtze University, Wuhan, 430113

{xianfengwu, yajingbai}@stu.jhun.edu.cn laizhy@jhun.edu.cn

{tianyulu, jsyuan}@buffalo.edu 02007847@yangtzeu.edu.cn

Abstract

While previous studies have demonstrated successful 3D object shape completion with a sufficient number of points, they often fail in scenarios when a few points, e.g. tens of points, are observed. Surprisingly, via entropy analysis, we find that even a few points, e.g. 64 points, could retain substantial information to help recover the 3D shape of the object. To address the challenge of shape completion with very sparse point clouds, we then propose Few-point Shape Completion (FSC) model, which contains a novel dual-branch feature extractor for handling extremely sparse inputs, coupled with an extensive branch for maximal point utilization with a saliency branch for dynamic importance assignment. This model is further bolstered by a two-stage revision network that refines both the extracted features and the decoder output, enhancing the detail and authenticity of the completed point cloud. Our experiments demonstrate the feasibility of recovering 3D shapes from a few points. The proposed Few-point Shape Completion (FSC) model outperforms previous methods on both few-point inputs and many-point inputs, and shows good generalizability to different object categories.

1. Introduction

Point-cloud-based shape completion is showing exciting prospects in applications such as autonomous driving, robotics, augmented reality, etc. Limited by the sensors'

*Equal contribution.

†Corresponding author. This work was supported by the National Key Research and Development Program of China (No. 2021YFC3100804), National Natural Science Foundation of China (No. 62106086), China Scholarship Council (No. 201908420105), Key Research and Development Program of Hubei Province (No. 2021BAD004), State Key Laboratory of Precision Blasting, Jiangnan University (No. PBSKL2022201), National Undergraduate Training Programs for Innovation and Entrepreneurship (Nos. 202311072004 and 202311072010), Undergraduate Research Programs of Jiangnan University (Nos. 2023zd111 and 2023zd117).



Figure 1. We use 64 points as input for point cloud completion. The PCN [57] result does not result in good general shapes. GRNet [51] result has unexpected holes due to the lack of dense representations. In comparison, our few-point shape completion method can provide much more reasonable results.

range and resolution, the point cloud the sensors generate can often be sparse, providing only a few points as input. This application scenario makes few-point shape completion critically important. However, compared to existing works that utilize a few thousand points as input, completing the point cloud with no more than a few dozen points not only faces the absence of local details in the input but more importantly, the highly compromised global shape information. This disparity makes the task of shape completion with such limited input even more challenging.

Despite the progress in point cloud-based shape completion highlighted in works like [1, 20, 31, 32, 35, 52, 57, 67], few have tackled the challenge of completing a point cloud with few input points. Previous works like [51, 57] typically utilize a few thousand points as input and demonstrate competent completion capabilities with this volume of input. However, these works do not investigate the potential for point cloud completion when the number of input points is significantly reduced, which scenario might arise in many practical applications. They do not explore the extent of the information contained in a few-point input or attempt to leverage this information to enhance point cloud completion. Previous studies like PCN [57] use feature encoders, often inspired by PointNet [24] or PointNet++ [26], for capturing input shape features. However, with a limited number of points, where each point is more crucial, the feature extraction must effectively use all points and prior-

itize their importance for diverse shape information. This ensures the feature quality from few-point inputs is on par with many-point inputs. Conversely, voxel-based methods like GRNet [51] may succeed in global shape recovery, but they face challenges in creating dense representations from a few points. Fig. 1 shows 64 points input results in inaccurate global shapes with PCN, while voxel-based approaches GRNet yield sparse outcomes.

To explore how much information that contained in the few-point input, we use Shannon Entropy [29] to evaluate the information when we randomly drop the points from input. We found that even when the input has only 64 randomly chosen points, it still contains nearly 50% of the ground truth shape information. To effectively recover global shape information and generate a comprehensive point cloud from sparse inputs, we designed a dual-branch feature extractor. The extensive branch ensures full utilization of each input point, while the saliency branch dynamically assigns importance to points based on their relevance. This design balances equitable point consideration with the flexibility to adjust point significance. Additionally, our two-stage revision network refines the extracted features and the output from the decoder, improving the output’s authenticity and detail for a more accurate point cloud.

Specifically, our Few-point Shape Completion (FSC) model contains two primary modules: recovery and revision. The recovery module employs an MLP-based branch for comprehensive feature extraction, utilizing a simple yet effective MLP-based design to fulfill our objective of extensive feature extraction. In the meantime, the salient feature extraction branch incorporates a transformer-based design, facilitating dynamic exploration of the importance of individual points. For the revision module, we leverage Wasserstein GAN (WGAN) to act upon both the latent feature and the point cloud results, with both WGAN generators being fashioned as simple MLPs. Our approach goes beyond utilizing WGAN solely for output point cloud enhancement; it also ensures that the global shape feature is closely aligned with the ground truth input feature generated from our recovery module, thereby improving the detailed shape of the point cloud. Additionally, we employ a PointNet-based module to decode the extracted feature into finely detailed point clouds.

Our contributions are as follows:

- We investigate the potential of completing point clouds with a few input points. This research gives a minimum of how many points would be enough to complete the entire point cloud.
- We present a solution named Few-point Shape Completion (FSC) model capable of completing a point cloud from a few sparse points. To our knowledge, our work is the first one that focuses on the few-point completion task.

- We design a dual-branch feature recovery architecture to separately capture the extensive and salient information. This dual-branch design equitably utilized the information of all points while adaptively adjusting the importance of each point.
- We design a two-stage revision module that uses WGAN directly on the feature space and on point cloud results. This two-stage revision ensures the global shape feature aligns more closely with that of the authentic point cloud while enhancing the shape.

Our experiments demonstrate that our method surpasses previous approaches with both many and few input points. We also verify that our method has good robustness to different input point numbers, unseen point cloud categories, and different randomized input points.

2. Related Work

2.1. Point-cloud-based Shape Completion

Point cloud completion [3, 6, 21, 22, 33, 34, 36, 38, 43, 46, 50, 58, 59, 61, 65] is a vital task in 3D computer vision with a multitude of applications, such as robot perception, autonomous driving, and augmented reality. Voxel-based and point-based methods are the two primary categories of point cloud completion approaches. The voxel-based method converts the input point cloud into voxels and subsequently generates complementary results in both voxel and point cloud representations. GRNet [51] exemplifies a voxel-based method that leverages 3D CNNs to extract voxel features and multilayer perceptrons (MLPs) to produce complementary results in point cloud representation. Nonetheless, voxel-based methods exhibit a lack of robustness when confronted with a limited number of input points, leading to missing voxel neighborhoods and, consequently, the generation of results containing holes.

In contrast, point-based methods directly perform point cloud completion on the input points. PCN [57], a trailblazing point-based method, segregates the completion process into an encoder and a decoder. The encoder utilizes PointNet to extract global features, while the decoder employs fully connected and FoldingNet networks to generate coarse and fine point clouds, respectively. Given that the completion process negates the need for neighborhood calculation, point-based methods are more resilient to variations in the number of input points. However, their completion outcomes are often suboptimal, prompting the advent of various enhancement methods such as PF-Net [14], TopNet [25], and SA-Net [62]. These methods concentrate on procuring more representative point clouds with distinct geometric features and progressively amplifying the resolution of the generated point cloud.

2.2. Point Cloud Analysis

Point cloud analysis encompasses a range of tasks including segmentation, object detection, registration, completion, and surface reconstruction, with deep learning-based methods, such as [13, 15, 17–19, 24, 40, 42, 54], being widely implemented. In these works, point clouds are typically encoded either by leveraging their connections with neighboring points, as seen in methods like PointNet++[26], DGCNN[40], and Point Transformer [63], or by employing simple networks such as MLP, as in the encoder of PCN [57]. While these encoding designs have proven to be effective in previous point cloud completion tasks, they tend to fall short when dealing with inputs comprising a limited number of points. Given this constraint of limited input information, our point cloud encoder must be significantly more effective than those employed in previous point cloud analysis approaches.

3. Few-point Information Analysis

We first analyze how many input points can provide enough information for completing the point cloud. To measure the information, we use Fast Point Feature Histograms (FPFH) Entropy in [12] to encode the shape and calculate its Shannon Entropy. FPFH of a point cloud is defined in [28]. FPFH is a widely used shape descriptor that encodes the shape of a point cloud into a histogram. Having this quantization, we can calculate the FPFH Entropy as

$$S = - \sum_i FPFH_i \log(FPFH_i), \quad (1)$$

where $FPFH_i$ is the i th bin of normalized FPFH.

Having FPFH entropy, we can calculate how much percentage of information has been lost when we reduce the number of points. We show in Fig. 3 the information reduction when the input number of points changes. We found that only 64 points input contains almost 50% of the shape information under a reasonable quantization level. In the next section, we try to design a solution that can complete the point cloud of 64 or more points.

4. Few-point Shape Completion

Our task is to design a point cloud completion network architecture that can take very few partial points as input. Specifically, given the vertex locations of the input point cloud $X \in R^{n \times 3}$ (n is the input point number), our network can be abstracted as:

$$Y = F(X), \quad (2)$$

where $Y \in R^{m \times 3}$ is the output point cloud and m is the output point number. Different from the previous point cloud

completion task that takes thousands of points as input, few-point completion would require a much smaller number of points. Typically, we would constrain the point number to no less than 64, *i.e.* $m \geq 64$.

4.1. Pipeline

Our Few-point Shape Completion (FSC) model uses an encoder-decoder architecture illustrated in Fig. 2a. This architecture consists of a dual-branch encoder that transforms the input point cloud into a latent feature space. The dual branches are specifically designed to extract both extensive and salient information from the point cloud. After extracting these features, a two-stage revision network is applied to enhance the feature quality. This revision process is set up adversarially, aiming to bring the point cloud result closer to an actual point cloud and align the features more closely with those derived from a real point cloud. This method improves both the features and the quality of the point cloud results. Subsequently, the revised features are fed into a decoder network to generate a detailed point cloud. The fusion of local and global representations of the point features is achieved using PointNet++[26] and multi-head external attention[11]. Finally, the FoldingNet approach [53] is employed to create the final detailed point cloud.

4.2. Dual-branch Feature Extraction

We focus on developing a feature extraction network that can effectively extract the coarse features f_{coarse} of point clouds X as

$$f_{\text{coarse}} = F_{\text{ext}}(X), \quad (3)$$

Our approach addresses the challenge of sparse feature extraction from point clouds with limited points. We employ a dual-branch feature extraction network, combining point-specific and global information. This includes a double-layer stacking technique for a richer representation and a transformer-based network to enhance global feature correlation. We balance detailed shape features with globally relevant ones, leveraging the strengths of PointNet[24] and PCN [57] methodologies. This results in a robust, effective solution for feature extraction in sparse point clouds.

Extensive branch. The extensive branch of the network has a structure that is similar to the PCN feature extraction network, which also utilizes a two-layer stacking architecture. In the first layer, the multilayer perceptron network takes the $n \times 3$ -dimensional sparse point cloud X as input to generate the feature matrix F_1^1 . Then, the feature vector f_1^1 is obtained through maximum pooling. In the second layer, the global features f_1^1 are merged into each row of the feature matrix F_1^1 , resulting in an expanded point feature matrix \tilde{F}_1^1 . Subsequently, the feature vector f_2^1 is generated by applying two multilayer perceptrons and maximum pooling sequentially. Finally, f_1^1 and f_2^1 are combined to form the feature vector f^1 of the first branch.

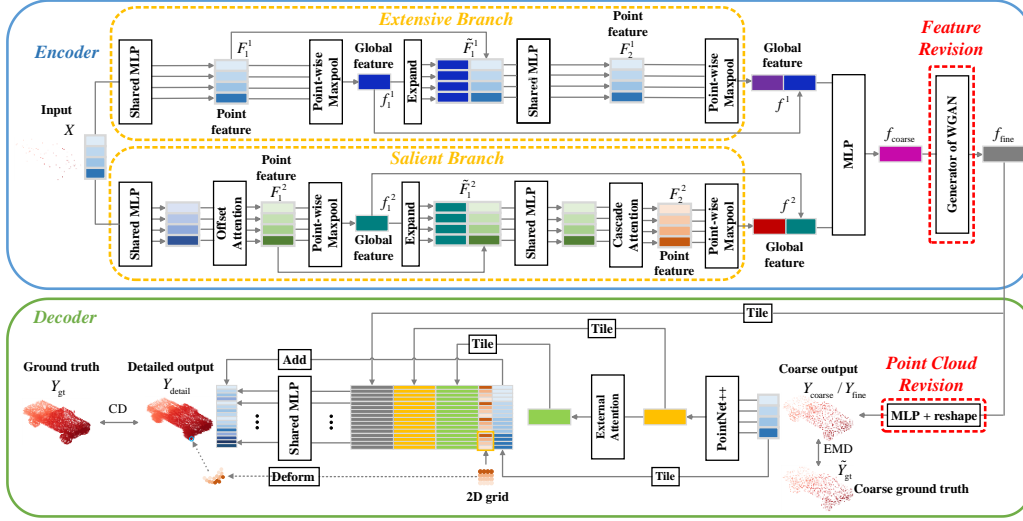


Figure 2. FSC pipeline. The dual-branch feature extraction network abstracts the input point cloud X as a rough feature vector f_{coarse} . The two-stage revision network corrects f_{coarse} and the coarse point cloud Y_{coarse} as f_{fine} and Y_{fine} , respectively. The detail point cloud Y_{detail} is generated by using f_{fine} , Y_{fine} and its point features.

Salient branch. The structure of the salient branch is similar to that of the first branch. However, it differs in that the second branch includes an offset attention module [10] inserted after the multilayer perceptron network in the first layer of the two-layer stacked structure. Additionally, a two-layer cascaded attention module [47] is inserted between the two multilayer perceptron networks in the second layer to enhance the global representation of the point features in the second layer. The goal of this modification is to improve the effectiveness of the feature extraction process for the salient branch. Finally, the coarse feature vector f_{coarse} is obtained by concatenating the feature vectors f^1 and f^2 of the two branches together.

4.3. Two-stage Revision

The two-stage revision network is used to correct the coarse feature vector f_{coarse} and the rough point cloud Y_{coarse} . As shown in Fig. 2, this process can be abstracted as:

$$\begin{aligned} f_{\text{fine}} &= F_{\text{rf}}(f_{\text{coarse}}), \\ Y_{\text{coarse}} &= \text{MLP}(f_{\text{fine}}), \\ Y_{\text{fine}} &= F_{\text{rp}}(Y_{\text{coarse}}), \end{aligned} \quad (4)$$

where f_{fine} is the revised feature using the first stage feature revision. Y_{coarse} is the resulting coarse point cloud getting from the revised feature. Y_{fine} is the shape revised point cloud with the same number of points as Y_{coarse} . F_{rf} and F_{rp} are the feature and point cloud revision network. In this process, we aim to generate a point cloud that is closer to the real point cloud and revise the feature to be more similar to the features generated from the real point cloud.

This adversarial approach leads to a better quality of both the feature and the point cloud results.

Specifically, our two-stage revision network refines both the coarse feature vector and the rough point cloud. In the first stage, a seven-layer fully connected generator adjusts the coarse feature vector, using feature fusion through layer stitching. An attention-enhanced four-layer discriminator network analyzes feature channel correlations. The second stage focuses on aligning the rough point cloud with the downsampled true point cloud, using a three-layer generator and a four-layer discriminator. This method effectively enhances the fidelity of both features and point clouds, ensuring they closely resemble those from real point clouds.

Finally, the decoder network is used to generate the detail point cloud output Y_{detail} from the shape revised point cloud Y_{fine} as

$$Y_{\text{detail}} = F_{\text{gd}}(Y_{\text{fine}}), \quad (5)$$

where F_{gd} is the detailed point cloud generation network.

4.4. Training Losses

The loss function is used to measure the difference between the output point cloud and the true point cloud. Similar to [57], this loss function L is defined as follows:

$$\begin{aligned} L(Y_{\text{coarse}}, Y_{\text{detail}}, Y_{\text{gt}}) &= \\ d_1(Y_{\text{coarse}}, \tilde{Y}_{\text{gt}}) &+ \alpha d_2(Y_{\text{detail}}, Y_{\text{gt}}) \end{aligned} \quad (6)$$

The above loss function consists of d_1 , d_2 , and weights α . d_1 and d_2 represent the distance between the output point cloud and the true value at the coarse level and the detail level, respectively.

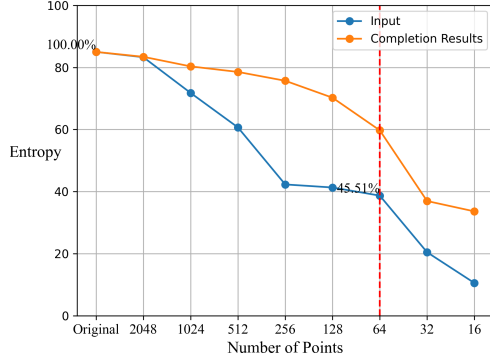


Figure 3. We analyze the FPFH Shannon Entropy of the input point cloud and completion results on ShapeNet. We observe that when the number of input points drops to 64, the input point cloud still contains 45.51% of the amount of information compared to the original 16,384 points (blue line). When the number of points further decreases, the amount of information drops sharply. In the experiment of this paper, we use 64 as the minimum number of points. The orange line shows the information of the point cloud after completion.

To ensure that the final output point cloud matches the true value in terms of both density distribution and overall structure, while keeping the computational effort low, we utilize two methods in our implementation. We use Earth Mover’s Distance (EMD) [27] for d_1 calculation, which involves fewer points but provides high-density consistency with high computational complexity. For d_2 calculation, we use Chamfer Distance (CD) [7], which involves more points but provides high structural consistency with low computational complexity. Specifically,

$$\begin{aligned}
 d_1(Y_{\text{coarse}}, \tilde{Y}_{\text{gt}}) &= \text{EMD}(Y_{\text{coarse}}, \tilde{Y}_{\text{gt}}) \\
 &= \min_{\phi: Y_{\text{coarse}} \rightarrow \tilde{Y}_{\text{gt}}} \frac{1}{|Y_{\text{coarse}}|} \sum_{p \in Y_{\text{coarse}}} \|p - \phi(p)\|_2. \quad (7)
 \end{aligned}$$

The above equation finds the bijection ϕ from Y_{coarse} to \tilde{Y}_{gt} such that the average distance between the output point and the corresponding real point is minimized.

$$\begin{aligned}
 d_2(Y_{\text{detail}}, Y_{\text{gt}}) &= \text{CD}(Y_{\text{detail}}, Y_{\text{gt}}) \\
 &= \frac{1}{|Y_{\text{detail}}|} \sum_{p \in Y_{\text{detail}}} \min_{q \in Y_{\text{gt}}} \|p - q\|_2 + \frac{1}{|Y_{\text{gt}}|} \sum_{q \in Y_{\text{gt}}} \min_{p \in Y_{\text{detail}}} \|q - p\|_2. \quad (8)
 \end{aligned}$$

The above symmetric form of the chamfer distance is used to calculate the average closest distance between the output point cloud and the real point cloud to ensure that they are covered by each other. More training details can be found in Supplementary Material Sec. 1.

5. Experiments

5.1. Data Generation and Datasets

ShapeNet data generation. We train and evaluate our method on ShapeNet [2]. It is a synthetic CAD dataset comprising 30,974 complete and detailed 3D point clouds. There are in total 16 categories of point clouds in ShapeNet. We use 8 of them for training and testing (“seen categories”), and use the other 8 categories (“unseen categories”) for the generalizability test. To simulate realistic input point clouds, we sample input point clouds from the mesh surface. Specifically, we first uniformly sample 16,384 points as Ground truth. Then, we generated partial point clouds with 2048 points by back-projecting 2.5D depth images into 3D. Subsequently, we downsampled these to create low-resolution partial point clouds with varying densities: 1024, 512, 256, 128, and 64 points. The entire dataset of 30,974 3D point clouds was divided into training (28,974 point clouds), validation (800 point clouds), and testing sets (1,200 point clouds). We use the same ($CD-\ell_1$) as in PCN [57] to evaluate our completion accuracy on both datasets. $CD-\ell_1$ is the Chamfer Distance using L1-norm, which is defined as

$$CD-\ell_1(\hat{P}, P) = \frac{1}{|\hat{P}|} \sum_{x \in \hat{P}} \min_{y \in P} \|x - y\|_1 + \frac{1}{|P|} \sum_{y \in P} \min_{x \in \hat{P}} \|x - y\|_1, \quad (9)$$

where \hat{P} and P are the completion and ground truth point clouds. x and y are points in \hat{P} and P , respectively. $|\cdot|$ is the size of a set, and $\|\cdot\|_1$ indicates the L1-norm. To be consistent with PCN, the number reported was multiplied by 1000 in experiments.

KITTI dataset. The KITTI [8] dataset is an in-the-wild benchmark dataset extensively used in autonomous driving and computer vision research, with a strong focus on LiDAR-based point clouds. It features a comprehensive collection of point cloud data captured from LiDAR sensors, providing detailed 3D representations of urban environments for vehicle and pedestrian detection, and scene understanding tasks. We evaluate our method on this dataset using Minimum Matching Distance (MMD) in [55] as the metric. MMD is defined as

$$\text{MMD}(\hat{P}, \mathbf{C}) = \min_{P \in \mathbf{C}} CD-\ell_2(\hat{P}, P), \quad (10)$$

$CD-\ell_2$ is the Chamfer Distance the output \hat{P} and the point cloud P from car category \mathbf{C} in ShapeNet that is closest to \hat{P} in terms of $CD-\ell_2$, where

$$CD-\ell_2(\hat{P}, P) = \frac{1}{|\hat{P}|} \sum_{x \in \hat{P}} \min_{y \in P} \|x - y\|_2^2 + \frac{1}{|P|} \sum_{y \in P} \min_{x \in \hat{P}} \|x - y\|_2^2, \quad (11)$$

To be consistent with [55], the number reported was multiplied by 1000 in experiments.

	Avg CD- ℓ_1 ↓	Airplane	Cabinet	Car	Chair	Lamp	Sofa	Table	Vassel
GRNet [51]	17.61	19.40	23.32	14.62	10.54	15.64	16.39	16.71	24.26
PoinTr [55]	13.68	10.53	15.72	12.59	13.84	14.59	15.45	14.70	11.98
PCN [57]	12.11	14.53	11.50	13.32	6.90	12.01	11.37	14.44	12.80
SeedFormer [64]	12.38	8.56	16.14	11.38	14.25	10.11	17.50	11.50	9.62
SVDFormer [66]	11.22	7.21	13.86	11.00	13.15	10.02	13.90	10.64	10.02
Ours	7.89	3.47	8.93	6.70	10.12	10.31	10.83	7.61	7.63

Table 1. 64 points completion accuracy on the 8 “seen categories” of ShapeNet. We can see that our method outperforms previous methods on average and in most categories. Avg CD- ℓ_1 the lower the better. **Bold** number means the best.

	Avg CD- ℓ_1 ↓	Airplane	Cabinet	Car	Chair	Lamp	Sofa	Table	Vessel	Methods	Avg CD- ℓ_2 ↓
3D-EPN [5]	20.15	13.16	21.80	20.31	18.81	25.75	21.09	21.712	18.54	PCN [57]	18.22
FoldingNet [53]	14.31	9.49	15.80	12.61	15.55	16.41	15.97	13.65	14.99	AtlasNet [9]	17.77
AtlasNet [9]	10.85	6.37	11.94	10.10	12.06	12.37	12.99	10.33	10.61	TopNet [25]	14.25
CRN [37]	11.98	6.44	15.09	13.75	12.37	11.38	14.70	11.78	10.33	SoftPoolNet [41]	11.07
MSN [16]	10.00	5.60	11.90	10.30	10.20	10.70	11.60	9.60	9.90	GRNet [51]	10.64
PCN [57]	9.64	5.50	10.63	8.70	11.00	11.34	11.68	8.59	9.67	PMP-Net [44]	9.23
TopNet [25]	9.89	6.24	11.63	9.83	11.50	9.37	12.35	9.36	8.85	PoinTr [55]	9.22
GRNet [51]	8.83	6.45	10.37	9.45	9.41	7.96	10.51	8.44	8.04	CRN [37]	9.21
PMP-Net [44]	8.66	5.50	11.10	9.62	9.47	6.89	10.74	8.77	7.19	SCRN [39]	9.13
PoinTr [55]	8.38	4.75	10.47	8.68	9.39	7.75	10.93	7.78	7.29	VRCNet [23]	8.12
SCRN [39]	8.29	4.80	9.94	9.31	8.78	8.66	9.74	7.20	7.91	PMP-Net++ [45]	7.97
NSFA [60]	8.06	4.76	10.18	8.63	8.53	7.03	10.53	7.35	7.48	Snowflake [49]	7.60
Snowflake [49]	7.21	4.29	9.16	8.08	7.89	6.07	9.23	6.55	6.40	ASFNet [48]	6.68
Ours	7.02	4.07	9.12	8.10	7.21	5.88	9.30	6.26	6.25	Ours	6.66

Table 2. 2048 points completion accuracy on the 8 “seen categories” of ShapeNet. We can see that our method outperforms previous methods in most categories and the average results.

Table 3. 2048 points completion accuracy on Completion3D.

Completion3D dataset. We also compare our results on Completion3D [30], which is another 3D object point cloud completion benchmark designed based on the data in ShapeNet. Here, we use the same $CD-\ell_2$ metric as defined in Eq. (11).

5.2. Shannon Information Analysis

We analyze the Shannon information for few-point inputs and completion results on ShapeNet. We use Eq. (1) in Sec. 3 to evaluate the FPFH Entropy of input point clouds. We set the voxel size of FPFH to approximately 2% of the point cloud’s overall size, meaning we do not take into consideration the errors that are smaller than that. The radius and bin count are set to 1cm and 36, respectively. The results are shown in Fig. 3. The blue line shows the entropy of different inputs and the orange line shows the results of the corresponding completed point cloud. Compared with the ground truth point cloud, our 64-point input has 45.51% information of the ground truth. We can also see from the orange line that even with 64-point input, we can also recover 60% of the shape information.

5.3. Results

Few-point results on ShapeNet. We train and evaluate our method on 8 categories of point clouds on ShapeNet. Tab. 1 presents the per-class completion results on ShapeNet for scenarios where the input point cloud contains only 64

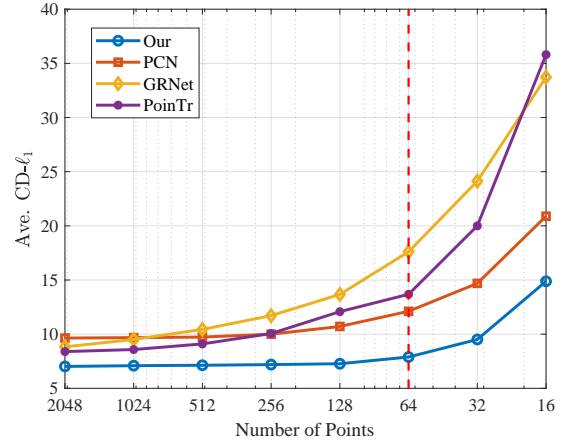


Figure 4. In our comparative analysis on ShapeNet, we varied the input point number from 2048 to 16. We observe that our model (blue line) consistently outperformed previous methods across different input point counts. Notably, when the number of input points was reduced to below 64, there was a significant decline in performance for all evaluated methods.

points. In all eight “seen categories”, our method outperforms others, achieving the highest accuracy. We observe a notable improvement over the previous method. This demonstrates that our approach has a distinct advantage in completion accuracy, especially in cases of few-point point

Methods	PCN [57]	NSFA [60]	CRN [37]	PFNet [14]	GRNet [51]	PoinTr [55]	SeedFormer [64]	AnchorFormer [4]	AdaPoinTr [56]	Ours
MMD↓	1.366	0.891	0.872	0.792	0.568	0.526	0.516	0.458	0.392	0.239

Table 4. Completion results on KITTI dataset with various number of input points.

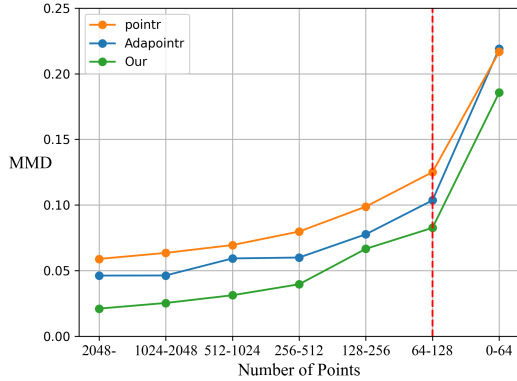


Figure 5. We report the completion result grouped by the number of input points on LiDAR scans of the KITTI dataset. As shown in the figure, our method (green line) outperforms previous methods in every number of input point groups. We also observe a sharp error increase when the number of input points is lower than 64.

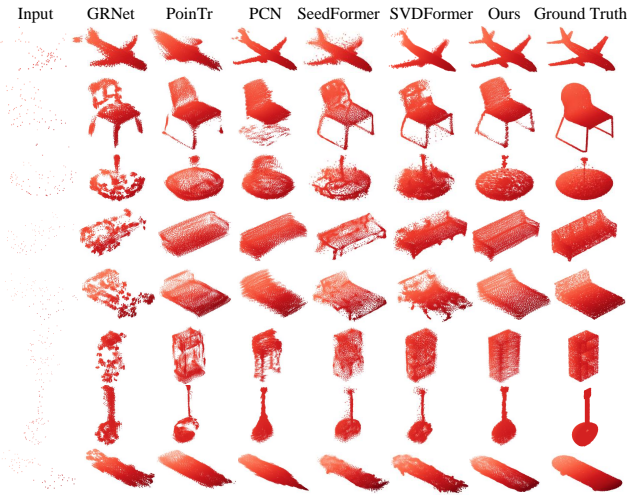


Figure 6. Visualized results for 64 input points. The top four rows are the results of categories used during training (“seen” categories). The bottom four rows are the results of categories not seen during training (“unseen” categories). As we can see, our method has better visualization results than previous methods.

cloud input. We also compare the performance on ShapeNet when the input point number varies from 2048 to 16 in Fig. 4. We can observe that our FSC outperforms previous approaches when the number of input points changes. Besides, when the number input point is less than 64, the performance of all methods drops sharply.

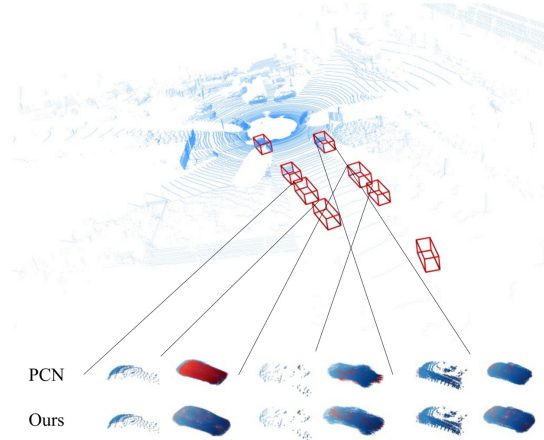


Figure 7. Visualization results compared on KITTI, Red and Blue are before after aligning the centroids of the point clouds.

Many-point results. In Tab. 2, we present the per-class completion results for scenarios with 2048 input points on ShapeNet, and in Tab. 3 on Completion3D. These results indicate that our method also outperforms previous approaches in cases of regular input point counts (2048).

Results on KITTI. We directly evaluate KITTI using the model trained on ShapeNet. As a real-world dataset, the input point number of KITTI varies from 1 to 2048. We first report the overall result on KITTI regardless of the input point number in Tab. 4. Our completion error is smaller than previous approaches. We also group the input point cloud in KITTI by the number of points to measure the performance when the input number of points varies. Our result is shown in Fig. 5. We can observe that our method outperforms previous approaches when the number of points drops. The experiments on KITTI show the generalizability of our method to different datasets.

Results on unseen categories of ShapeNet. Tab. 5 gives the per-class completion results for the shape from unseen categories when the input point cloud only contains 64 points. Our method still achieves the best performance in all 8 unknown categories. This experiment shows our method has reasonable generalizability to unseen objects.

Ablation studies. Tab. 6 gives the contribution of each module to the performance improvement under different numbers of input points, respectively. No matter how many input points there are and what we choose, using the salient branch instead of the extensive branch can always improve the completion accuracy, and by combining the two branches together, the accuracy can be further improved. This justifies our design of dual-branch feature extraction

	Avg CD- ℓ_1 ↓	Bus	Bed	Bookshelf	Bench	Guitar	Motorbike	Skateboard	Pistol
GRNet [51]	17.03	17.59	25.61	21.93	15.26	10.85	14.83	14.96	15.17
PCN [57]	15.52	11.30	25.86	16.22	12.55	11.47	15.30	13.48	17.95
PoinTr [55]	14.92	14.62	20.44	16.84	14.22	11.56	13.40	14.45	13.80
SVDFormer [66]	13.60	13.30	21.47	13.73	11.69	8.00	13.25	9.91	17.44
Ours	12.90	7.94	22.60	12.98	9.59	9.77	13.56	11.55	14.92

Table 5. Results for 64 points on shapes from unseen categories in ShapeNet. We observe that even on unseen categories, we can still have reasonable results, and our method still outperforms previous methods on average and most unseen categories.

	Module							Number of input points					
	Extensive branch Baseline Encoder	Saliency branch	Feature revision	Point cloud revision	PointNet++	Transformer	Decoder Baseline Decoder	2048	1024	512	256	128	64
a	✓						✓	9.64	9.68	9.73	10.00	10.71	12.11
b		✓					✓	8.66	8.71	8.76	8.95	9.42	10.53
c	✓	✓					✓	8.31	8.35	8.42	8.49	8.59	9.78
d	✓		✓				✓	8.33	8.39	8.43	8.60	9	10
e	✓			✓			✓	9.01	9.11	9.18	9.27	10.07	11.35
f	✓		✓	✓			✓	8.01	8.07	8.15	8.29	8.55	9.14
g	✓				✓		✓	9.31	9.36	9.41	9.65	10.28	11.58
h	✓					✓	✓	8.91	8.99	9.08	9.17	9.72	11.02
i	✓				✓	✓	✓	8.5	8.58	8.66	9.02	9.43	11.24
j	✓		✓	✓	✓	✓	✓	7.97	8.03	8.07	8.22	8.51	9.46
k		✓	✓	✓	✓	✓	✓	7.35	7.41	7.46	7.54	7.7	8.42
Ours	✓	✓	✓	✓	✓	✓	✓	7.02	7.09	7.13	7.19	7.27	7.89

Table 6. Ablation study under different numbers of input points. Our performance decreases when we remove some necessary modules.

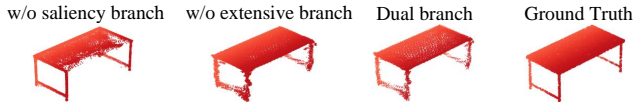


Figure 8. Visualized comparison of removing each branch in feature extractor. From left to right: removing saliency branch, removing extensive branch, keeping both branch (proposed method), and Ground Truth.

and the two-stage revision network. We also show an visualized example of removing one of feature extraction dual branches in Fig. 8. Our proposed method (third one from the left) achieves the best results.

Visualizations. Fig. 6 shows visualized results on ShapeNet. The input point cloud only contains 64 points. As we can see, GRNet [51] may only generate some non-connected clusters around isolated input points, whereas the category information may be completely lost. Although PCN [57] can generate connectivity, the results often contain large deformation and noise, leading to either difficulty or error in recognition. Although our method also contains deformation and noise, most of them are within an acceptable range. This illustrates the effectiveness of our method for the very low-resolution case. Besides, our visualized result on KITTI shows a similar result in Fig. 7.

Visualized result when input point number changes. Fig. 9 gives the completion results of an airplane when the number of input points gradually decreases from 2048 to 16. As the number of input points decreases, our method always recovers a better point cloud, which further illus-

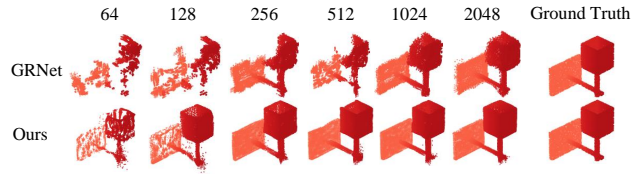


Figure 9. Qualitative completion results of a lamp when the number of points increases from 64 to 2048. Our visualization results outperform GRNet for different numbers of points.

trates our stability against the variations in the number of points of the input.

6. Conclusion

We have proposed a point cloud complementation network specifically for the case of very few points. To overcome the problem of missing neighborhood information due to very few points, we select a PCN that does not rely on neighborhood information in the encoding phase as the backbone network and combine a series of methods applicable to the very few points cases to enhance the overall performance of the complementation network. These specialized designs include 1) a dual-branch feature extraction network, 2) a two-stage revision network, and 3) a detailed point generation network with fused point features. Experimental results show that our method has a significant performance improvement over existing methods in very few point cases. Also, our method has good robustness for the shapes from unseen categories and the number of different points.

References

- [1] Panos Achlioptas, Olga Diamanti, Ioannis Mitliagkas, and Leonidas Guibas. Learning shape completion from point clouds using 3d generative adversarial networks. In *Proceedings of the IEEE Conference on Computer Vision and Pattern Recognition*, pages 2772–2776, 2017. 1
- [2] Angel X. Chang, Thomas Funkhouser, Leonidas Guibas, Pat Hanrahan, Qixing Huang, Zimo Li, Silvio Savarese, Manolis Savva, Shuran Song, Hao Su, Jianxiong Xiao, Li Yi, and Fisher Yu. Shapenet: An information-rich 3d model repository, 2015. 5
- [3] Chuanchuan Chen, Dongrui Liu, Changqing Xu, and Trieu-Kien Truong. Genecgan: A conditional generative adversarial network based on genetic tree for point cloud reconstruction. *Neurocomputing*, 462:46–58, 2021. 2
- [4] Zhikai Chen, Fuchen Long, Zhaofan Qiu, Ting Yao, Wengang Zhou, Jiebo Luo, and Tao Mei. Anchorformer: Point cloud completion from discriminative nodes. In *2023 IEEE/CVF Conference on Computer Vision and Pattern Recognition (CVPR)*, pages 13581–13590, 2023. 7
- [5] Angela Dai, Charles Qi, and Matthias Nießner. Shape completion using 3d-encoder-predictor cnns and shape synthesis. In *Proceedings of the IEEE conference on computer vision and pattern recognition*, pages 5868–5877, 2017. 6
- [6] Vage Egiazarian, Savva Ignatyev, Alexey Artemov, Oleg Voynov, Andrey Kravchenko, Youyi Zheng, Luiz Velho, and Evgeny Burnaev. Latent-space laplacian pyramids for adversarial representation learning with 3d point clouds. *ArXiv*, abs/1912.06466, 2019. 2
- [7] Haoqiang Fan, Hao Su, and Leonidas J Guibas. A point set generation network for 3d object reconstruction from a single image. In *Proceedings of the IEEE conference on computer vision and pattern recognition*, pages 605–613, 2017. 5
- [8] Andreas Geiger, Philip Lenz, and Raquel Urtasun. Are we ready for autonomous driving? the kitti vision benchmark suite. In *2012 IEEE Conference on Computer Vision and Pattern Recognition*, pages 3354–3361, 2012. 5
- [9] Thibault Groueix, Matthew Fisher, Vladimir G. Kim, Bryan C. Russell, and Mathieu Aubry. A papier-mâché approach to learning 3d surface generation. In *Proceedings of the IEEE/CVF Conference on Computer Vision and Pattern Recognition (CVPR)*, pages 216–224, 2018. 6
- [10] Meng-Hao Guo, Jun-Xiong Cai, Zheng-Ning Liu, Tai-Jiang Mu, Ralph R Martin, and Shi-Min Hu. Pct: Point cloud transformer. *Computational Visual Media*, 7:187–199, 2021. 4
- [11] Meng-Hao Guo, Zheng-Ning Liu, Tai-Jiang Mu, and Shi-Min Hu. Beyond self-attention: External attention using two linear layers for visual tasks. *IEEE Transactions on Pattern Analysis and Machine Intelligence*, pages 1–13, 2022. 3
- [12] Chenming Hu, Yu Ru, Shuping Fang, Hongping Zhou, Jiangkun Xue, Yuheng Zhang, Jianping Li, Guopeng Xu, and Gaoming Fan. A tree point cloud simplification method based on fpfh information entropy. *Forests*, 14(7):1507, 2023. 3
- [13] Hengshuang Hu, Yangyan Li, and Xiaolin Li. Part attention pointnet for fine-grained point cloud classification. In *Proceedings of the IEEE/CVF Conference on Computer Vision and Pattern Recognition (CVPR)*, pages 14972–14981, 2021. 3
- [14] Zitian Huang, Yikuan Yu, Jiawen Xu, Feng Ni, and Xinyi Le. PF-net: Point fractal network for 3d point cloud completion. In *Proceedings of the IEEE/CVF Conference on Computer Vision and Pattern Recognition (CVPR)*, pages 7662–7670, 2020. 2, 7
- [15] Chenyang Jiang, Bin Zhang, Hao Li, Jian Wang, and Yong Liu. Point-wise convolutional neural networks for high-resolution 3d point cloud analysis. *IEEE Transactions on Pattern Analysis and Machine Intelligence (TPAMI)*, 42(5):1272–1284, 2019. 3
- [16] Minghua Liu, Lu Sheng, Sheng Yang, Jing Shao, and Shi-Min Hu. Morphing and sampling network for dense point cloud completion. *Proceedings of the AAAI Conference on Artificial Intelligence*, 34(07):11596–11603, 2020. 6
- [17] Tianyu Luan, Yali Wang, Junhao Zhang, Zhe Wang, Zhipeng Zhou, and Yu Qiao. Pc-hmr: Pose calibration for 3d human mesh recovery from 2d images/videos. In *Proceedings of the AAAI Conference on Artificial Intelligence*, pages 2269–2276, 2021. 3
- [18] Tianyu Luan, Yuanhao Zhai, Jingjing Meng, Zhong Li, Zhang Chen, Yi Xu, and Junsong Yuan. High fidelity 3d hand shape reconstruction via scalable graph frequency decomposition. In *Proceedings of the IEEE/CVF Conference on Computer Vision and Pattern Recognition*, pages 16795–16804, 2023.
- [19] Tianyu Luan, Zhong Li, Lele Chen, Xuan Gong, Lichang Chen, Yi Xu, and Junsong Yuan. Spectrum auc difference (saucd): Human-aligned 3d shape evaluation. *arXiv preprint arXiv:2403.01619*, 2024. 3
- [20] Yiwen Luo and Qixing Huang. Weakly supervised 3d point cloud completion in real time. *arXiv preprint arXiv:2004.08751*, 2020. 1
- [21] Yinyu Nie, Yiqun Lin, Xiaoguang Han, Shihui Guo, Jian Chang, Shuguang Cui, and Jian Jun Zhang. Skeleton-bridged point completion: From global inference to local adjustment. *arXiv preprint arXiv:2010.07428*, 2020. 2
- [22] Liang Pan. Ecg: Edge-aware point cloud completion with graph convolution. *IEEE Robotics and Automation Letters*, 5:4392–4398, 2020. 2
- [23] Liang Pan, Xinyi Chen, Zhongang Cai, Junzhe Zhang, Haiyu Zhao, Shuai Yi, and Ziwei Liu. Variational relational point completion network. *CoRR*, abs/2104.10154, 2021. 6
- [24] Charles R Qi, Hao Su, Kaichun Mo, and Leonidas J Guibas. Pointnet: Deep learning on point sets for 3d classification and segmentation. In *Proceedings of the IEEE conference on computer vision and pattern recognition*, pages 652–660, 2017. 1, 3
- [25] Charles Ruizhongtai Qi, Hao Su, Kaichun Mo, and Leonidas J Guibas. Topnet: Topology based neural network architecture search for 3d point cloud classification. In *Proceedings of the IEEE Conference on Computer Vision and Pattern Recognition*, pages 7224–7233, 2017. 2, 6
- [26] Charles R Qi, Li Yi, Hao Su, and Leonidas J Guibas. Pointnet++: Deep hierarchical feature learning on point sets in a

- metric space. In *Advances in Neural Information Processing Systems*, pages 5099–5108, 2017. 1, 3
- [27] Yossi Rubner, Carlo Tomasi, and Leonidas J Guibas. The earth mover’s distance as a metric for image retrieval. *International journal of computer vision*, 40(2):99, 2000. 5
- [28] Radu Bogdan Rusu, Nico Blodow, and Michael Beetz. Fast point feature histograms (fpfh) for 3d registration. In *2009 IEEE international conference on robotics and automation*, pages 3212–3217. IEEE, 2009. 3
- [29] Mark P Silverman. Cheating or coincidence? statistical method employing the principle of maximum entropy for judging whether a student has committed plagiarism. 2015. 2
- [30] Lyne P Tchapmi, Vineet Kosaraju, Hamid Rezatofighi, Ian Reid, and Silvio Savarese. Topnet: Structural point cloud decoder. In *Proceedings of the IEEE/CVF conference on computer vision and pattern recognition*, pages 383–392, 2019. 6
- [31] Hao Wang, Srinath Sridharan, Weixin Huang, Li Li, Rongjie Li, Zhichao Li, Tianfu Li, and Shuang Li. 3d point cloud completion with multimodal deep autoencoders. In *Proceedings of the European Conference on Computer Vision*, pages 641–656, 2018. 1
- [32] Haowen Wang, Zihao Zhu, Jianzhuang Lin, and Guoping Zhang. Deep global registration for point cloud completion. In *Proceedings of the IEEE Conference on Computer Vision and Pattern Recognition*, pages 2423–2432, 2019. 1
- [33] Jun Wang, Yinghan Cui, Dongyan Guo, Junxia Li, Qingshan Liu, and Chunhua Shen. Pointattn: You only need attention for point cloud completion. *ArXiv*, abs/2203.08485, 2022. 2
- [34] Kaiqi Wang, Ke Chen, and Kui Jia. Deep cascade generation on point sets. In *International Joint Conference on Artificial Intelligence*, 2019. 2
- [35] Xinxin Wang, Zizheng Zheng, Shu Liu, Jian Cao, and Zhaopeng Zhu. 3d point cloud completion with graph convolutional autoencoders. In *Proceedings of the IEEE Conference on Computer Vision and Pattern Recognition*, pages 5247–5256, 2019. 1
- [36] Xiaogang Wang, Marcelo H. Ang, and Gim Hee Lee. Point cloud completion by learning shape priors. *2020 IEEE/RSJ International Conference on Intelligent Robots and Systems (IROS)*, pages 10719–10726, 2020. 2
- [37] Xiaogang Wang, Marcelo H Ang Jr, and Gim Hee Lee. Cascaded refinement network for point cloud completion. In *Proceedings of the IEEE/CVF Conference on Computer Vision and Pattern Recognition*, pages 790–799, 2020. 6, 7
- [38] Xiaogang Wang, Marcelo H Ang, and Gim Hee Lee. Voxel-based network for shape completion by leveraging edge generation. In *2021 IEEE/CVF International Conference on Computer Vision (ICCV)*, pages 13169–13178, 2021. 2
- [39] Xiaogang Wang, Marcelo H Ang, and Gim Hee Lee. Cascaded refinement network for point cloud completion with self-supervision. *IEEE Transactions on Pattern Analysis and Machine Intelligence*, 44(11):8139–8150, 2021. 6
- [40] Yue Wang, Yongbin Sun, Ziwei Liu, Sanjay E Sarma, Michael M Bronstein, and Justin M Solomon. Dynamic graph cnn for learning on point clouds. *ACM Transactions on Graphics (TOG)*, 38(5):1–12, 2019. 3
- [41] Yida Wang, David Joseph Tan, Nassir Navab, and Federico Tombari. Softpoolnet: Shape descriptor for point cloud completion and classification. In *Computer Vision—ECCV 2020: 16th European Conference, Glasgow, UK, August 23–28, 2020, Proceedings, Part IX*, pages 70–85. Springer, 2020. 6
- [42] Ying Wei and Qixing Huang. Adaptive point cloud denoising with deep feature regularization. In *Proceedings of the IEEE/CVF Conference on Computer Vision and Pattern Recognition*, pages 12304–12313, 2020. 3
- [43] Xin Wen, Zhizhong Han, Yan-Pei Cao, Pengfei Wan, Wen Zheng, and Yu-Shen Liu. Cycle4completion: Unpaired point cloud completion using cycle transformation with missing region coding. In *2021 IEEE/CVF Conference on Computer Vision and Pattern Recognition (CVPR)*, pages 13075–13084, 2021. 2
- [44] Xin Wen, Peng Xiang, Zhizhong Han, Yan-Pei Cao, Pengfei Wan, Wen Zheng, and Yu-Shen Liu. Pmp-net: Point cloud completion by learning multi-step point moving paths. In *Proceedings of the IEEE/CVF conference on computer vision and pattern recognition*, pages 7443–7452, 2021. 6
- [45] Xin Wen, Peng Xiang, Zhizhong Han, Yan-Pei Cao, Pengfei Wan, Wen Zheng, and Yu-Shen Liu. Pmp-net++: Point cloud completion by transformer-enhanced multi-step point moving paths. pages 852–867, 2023. 6
- [46] Hang Wu and Yubin Miao. Cross-regional attention network for point cloud completion. In *2020 25th International Conference on Pattern Recognition (ICPR)*, pages 10274–10280, 2021. 2
- [47] Xianfeng Wu, Xinyi Liu, Junfei Wang, Zhongyuan Lai, Jing Zhou, and Xia Liu. Point cloud classification based on transformer. *Computers and Electrical Engineering*, 104:108413, 2022. 4
- [48] Yaqi Xia, Yan Xia, Wei Li, Rui Song, Kailang Cao, and Uwe Stilla. Asfm-net: Asymmetrical siamese feature matching network for point completion. pages 1938–1947, 2021. 6
- [49] Peng Xiang, Xin Wen, Yu-Shen Liu, Yan-Pei Cao, Pengfei Wan, Wen Zheng, and Zhizhong Han. Snowflakenet: Point cloud completion by snowflake point deconvolution with skip-transformer. In *Proceedings of the IEEE/CVF international conference on computer vision*, pages 5499–5509, 2021. 6
- [50] Chulin Xie, Chuxin Wang, Bo Zhang, Hao Yang, Dong Chen, and Fang Wen. Style-based point generator with adversarial rendering for point cloud completion. In *2021 IEEE/CVF Conference on Computer Vision and Pattern Recognition (CVPR)*, pages 4617–4626, 2021. 2
- [51] Haozhe Xie, Hongxun Yao, Shangchen Zhou, Jiageng Mao, Shengping Zhang, and Wenxiu Sun. Grnet: Gridding residual network for dense point cloud completion. In *Computer Vision—ECCV 2020: 16th European Conference, Glasgow, UK, August 23–28, 2020, Proceedings, Part IX*, pages 365–381. Springer, 2020. 1, 2, 6, 7, 8
- [52] Jie Yang, Zhe Zhao, Tao Wang, and Yang Liu. Context-aware completion of 3d part assemblies with shape-guided tree parsing. In *Proceedings of the IEEE Conference on Computer Vision and Pattern Recognition (CVPR)*, pages 7121–7129, 2018. 1

- [53] Yaoqing Yang, Chen Feng, Yiru Shen, and Dong Tian. Fold-ingnet: Point cloud auto-encoder via deep grid deformation. In *2018 IEEE/CVF Conference on Computer Vision and Pattern Recognition*, pages 206–215, 2018. [3](#), [6](#)
- [54] Yibo Yang, Chen Feng, Yi Shen, and Dong Tian. Point-flownet: Learning representations for rigid motion estimation from point clouds. In *Proceedings of the IEEE/CVF Conference on Computer Vision and Pattern Recognition (CVPR)*, pages 8264–8273, 2020. [3](#)
- [55] Xumin Yu, Yongming Rao, Ziyi Wang, Zuyan Liu, Jiwen Lu, and Jie Zhou. Pointr: Diverse point cloud completion with geometry-aware transformers. In *Proceedings of the IEEE/CVF international conference on computer vision*, pages 12498–12507, 2021. [5](#), [6](#), [7](#), [8](#)
- [56] Xumin Yu, Yongming Rao, Ziyi Wang, Jiwen Lu, and Jie Zhou. Adapointr: Diverse point cloud completion with adaptive geometry-aware transformers. *IEEE Transactions on Pattern Analysis and Machine Intelligence*, PP:1–17, 2023. [7](#)
- [57] Wentao Yuan, Tejas Khot, David Held, Christoph Mertz, and Martial Hebert. Pcn: Point completion network. In *2018 international conference on 3D vision (3DV)*, pages 728–737. IEEE, 2018. [1](#), [2](#), [3](#), [4](#), [5](#), [6](#), [7](#), [8](#)
- [58] Junzhe Zhang, Xinyi Chen, Zhongang Cai, Liang Pan, Haiyu Zhao, Shuai Yi, Chai Kiat Yeo, Bo Dai, and Chen Change Loy. Unsupervised 3d shape completion through gan inversion. In *2021 IEEE/CVF Conference on Computer Vision and Pattern Recognition (CVPR)*, pages 1768–1777, 2021. [2](#)
- [59] Wenxiao Zhang, Qingan Yan, and Chunxia Xiao. Detail preserved point cloud completion via separated feature aggregation. In *Computer Vision – ECCV 2020*, pages 512–528. Springer International Publishing, 2020. [2](#)
- [60] Wenxiao Zhang, Qingan Yan, and Chunxia Xiao. Detail preserved point cloud completion via separated feature aggregation. In *Computer Vision–ECCV 2020: 16th European Conference, Glasgow, UK, August 23–28, 2020, Proceedings, Part XXV 16*, pages 512–528. Springer, 2020. [6](#), [7](#)
- [61] Xuancheng Zhang, Yutong Feng, Siqi Li, Changqing Zou, Hai Wan, Xibin Zhao, Yandong Guo, and Yue Gao. View-guided point cloud completion. In *2021 IEEE/CVF Conference on Computer Vision and Pattern Recognition (CVPR)*, pages 15885–15894, 2021. [2](#)
- [62] Hengshuang Zhao, Li Zhang, Ji Liu, Tianwei Shi, Yingying Xia, and Xiaogang He. 3d point cloud segmentation with self-attention and group convolutional neural network. In *Proceedings of the IEEE Conference on Computer Vision and Pattern Recognition*, pages 9361–9370, 2019. [2](#)
- [63] Hengshuang Zhao, Li Jiang, Jiaya Jia, Philip Torr, and Vladlen Koltun. Point transformer. In *Proceedings of the IEEE/CVF International Conference on Computer Vision (ICCV)*, pages 16259–16268, 2021. [3](#)
- [64] Haoran Zhou, Yun Cao, Wenqing Chu, Junwei Zhu, Tong Lu, Ying Tai, and Chengjie Wang. Seedformer: Patch seeds based point cloud completion with upsample transformer. In *Computer Vision – ECCV 2022: 17th European Conference, Tel Aviv, Israel, October 23–27, 2022, Proceedings, Part III*, page 416–432, Berlin, Heidelberg, 2022. Springer-Verlag. [6](#), [7](#)
- [65] Liping Zhu, Bingyao Wang, Gangyi Tian, Wenjie Wang, and Chengyang Li. Towards point cloud completion: Point rank sampling and cross-cascade graph cnn. *Neurocomputing*, 461:1–16, 2021. [2](#)
- [66] Zhe Zhu, Honghua Chen, Xing He, Weiming Wang, Jing Qin, and Mingqiang Wei. Svdformer: Complementing point cloud via self-view augmentation and self-structure dual-generator. In *Proceedings of the IEEE/CVF International Conference on Computer Vision (ICCV)*, pages 14508–14518, 2023. [6](#), [8](#)
- [67] Daoming Zong, Shiliang Sun, and Jing Zhao. Ashf-net: Adaptive sampling and hierarchical folding network for robust point cloud completion. In *AAAI Conference on Artificial Intelligence*, 2021. [1](#)